Biochemical and Biophysical Research Communications 604 (2022) 57–62

Contents lists available at ScienceDirect

Biochemical and Biophysical Research Communications

journal homepage: www.elsevier.com/locate/ybbrc

Small integral membrane protein 10 like 1 downregulation enhances differentiation of adipose progenitor cells

Michèle Nebe [a], Stephanie Kehr [b], Samuel Schmitz [c], Jana Breitfeld [d], Judith Lorenz [a], Diana Le Duc [e, f], Peter F. Stadler [b, g], Jens Meiler [c, h], Wieland Kiess [a], Antje Garten [a], Anna S. Kirstein [a, *]

[a] University Hospital for Children & Adolescents, Center for Pediatric Research, Leipzig University, Leipzig, Germany
[b] Bioinformatics Group, Department of Computer Science and Interdisciplinary Center for Bioinformatics, Leipzig University, Leipzig, Germany
[c] Department of Chemistry, Vanderbilt University, Nashville, TN, USA
[d] Medical Department III-Endocrinology, Nephrology, Rheumatology, Leipzig University Medical Center, Leipzig, Germany
[e] Institute of Human Genetics, Leipzig University Medical Center, Leipzig, Germany
[f] Department of Evolutionary Genetics, Max Planck Institute for Evolutionary Anthropology, Leipzig, Germany
[g] Max Planck Institute for Mathematics in the Sciences, Leipzig, Germany
[h] Institute of Drug Discovery, Faculty of Medicine, Leipzig University, Leipzig, Germany

ARTICLE INFO

Article history:
Received 13 February 2022
Accepted 2 March 2022
Available online 4 March 2022

Keywords:
PTEN Hamartoma tumor syndrome
PHTS
Lipomatosis
Adipogenesis
SMIM10L1

ABSTRACT

Small integral membrane protein 10 like 1 (SMIM10L1) was identified by RNA sequencing as the most significantly downregulated gene in Phosphatase and Tensin Homologue (PTEN) knockdown adipose progenitor cells (APCs). PTEN is a tumor suppressor that antagonizes the growth promoting Phosphoinositide 3-kinase (PI3K)/AKT/mechanistic Target of Rapamycin (mTOR) cascade. Diseases caused by germline pathogenic variants in *PTEN* are summarized as PTEN Hamartoma Tumor Syndrome (PHTS). This overgrowth syndrome is associated with lipoma formation, especially in pediatric patients. The mechanisms underlying this adipose tissue dysfunction remain elusive. We observed that *SMIM10L1* downregulation in APCs led to an enhanced adipocyte differentiation in two- and three-dimensional cell culture and increased expression of adipogenesis markers. Furthermore, *SMIM10L1* knockdown cells showed a decreased expression of PTEN, pointing to a mutual crosstalk between PTEN and SMIM10L1. In line with these observations, *SMIM10L1* knockdown cells showed increased activation of PI3K/AKT/mTOR signaling and concomitantly increased expression of the adipogenic transcription factor SREBP1. We computationally predicted an α-helical structure and membrane association of SMIM10L1. These results support a specific role for SMIM10L1 in regulating adipogenesis, potentially by increasing PI3K/AKT/mTOR signaling, which might be conducive to lipoma formation in pediatric patients with PHTS.

1. Introduction

PHTS is caused by germline pathogenic variants in the tumor suppressor gene *PTEN*, a lipid and protein phosphatase, which functions as the main antagonist of the phosphoinositide 3-kinase (PI3K)/AKT/mechanistic Target of Rapamycin (mTOR) signaling pathway. PTEN dephosphorylates the second messenger phosphatidylinositol-3,4,5-trisphosphate (PIP3) and thereby reverses the action of PI3K. PI3K is activated by extracellular signals like insulin and leads to a downstream activation of AKT and mTOR, promoting cell growth, proliferation and survival. Patients with PHTS show a wide spectrum of clinical appearances for example neurodevelopmental abnormalities, malignancies such as breast, thyroid, renal and endometrial cancer or nonmalignant manifestations such as dermatologic features, gastrointestinal polyposis and vascular malformations. Bannayan-Riley-Ruvalcaba-type PHTS patients are predisposed to lipoma development [1]. We previously reported on a pediatric PHTS patient with progredient cachexia, multiple solitary lipomas and abdominal lipomatosis [2]. The pathogenesis of PHTS associated lipoma development is not clarified yet. Lipomatosis not only compromises the quality of life of

* Corresponding author. Leipzig University, Hospital for Children and Adolescents, Center for Pediatric Research Leipzig, Liebigstraße 21, 04103, Leipzig, Germany
E-mail address: anna.kirstein@medizin.uni-leipzig.de (A.S. Kirstein).

https://doi.org/10.1016/j.bbrc.2022.03.014

PHTS patients but can be harmful due to possible infiltration and displacement of surrounding organs and tissue. To investigate possible mechanisms for lipoma formation, we previously used adipose progenitor cells (APCs) isolated from human visceral adipose tissue to establish an *in vitro* model for PTEN haploinsufficiency [3]. RNA sequencing of APC with and without PTEN knockdown (KD) revealed 1379 differently expressed genes [3] (Supplementary Fig. 1). *SMIM10L1* was identified as the most significantly downregulated gene besides *PTEN*. It belongs to a family of small integral membrane proteins. The structure and function of this 68 amino acid protein with a calculated mass of 7.4 kDa are unknown. The *SMIM10L1* gene is located on the short arm of chromosome 12 and expression displays low tissue specificity [4,5]. SMIM10, another family member, is a mitochondrial membrane protein and was found to regulate BRAFV600E RNA and protein expression on a post-transcriptional level. BRAFV600E is a pathogenic variant of a Ser-Thr protein kinase and is known to be deleterious in various types of cancer. BRAFV600E melanoma cells transfected with SMIM10 undergo senescence and show a reduced proliferation, whereby the sensitivity to the BRAF-kinase inhibitor Vemurafenib is elevated. In addition, patients suffering from melanoma skin cancer expressing higher levels of SMIM10 have a better prognosis. These results suggest an oncosuppressive role for SMIM10 [6]. Two other gene family members, SMIM10L2A and SMIM10L2B, were identified as long non-coding RNAs that are positively associated with overall survival of patients with gastric cancer, suggesting them to be prognostic factors [7].

We aim to functionally characterize SMIM10L1 and its role in APCs and to investigate whether this protein could contribute to lipoma formation in PHTS patients.

2. Materials and methods

2.1. Computational structural characterization of SMIM10L1

The Rosetta membrane *ab-initio* protocol [8] was used to generate 20,000 models of the *SMIM10L1* gene product. All models were clustered with durandal [9], and the ten top scoring structures in each cluster were further analyzed with our custom Rosetta membrane scanning technique [10]. For that, we translated the model along the membrane z-axis in 1 Å increments and sampled 100 random rigid body perturbations for each membrane depth. The final model was selected by three criteria: I) the best Rosetta energy score, II) its agreement with Jufo9D [11] secondary structure prediction and III) plausible localization in the membrane. The secondary structure of the final model was visualized with POLYVIEW [12]. For visualization purposes, the CHARMM-GUI web toolkit [13] was used to generate an explicit membrane model as described in a previous study [14].

2.2. Integration of additional transcriptome data

For a broader understanding of the role of SMIM10L1 we integrated additional transcriptome data from a PTEN knockdown RNA Sequencing study [3] (Supplementary Fig. 1 and 1c) and differentiation of mouse adipocytes [15] (Supplementary Fig. 3b). Additional visualizations of these data were realized with programming language R [16].

2.3. Cell culture

We obtained APCs from the stromal vascular fraction (SVF) of visceral adipose tissue extracted from three healthy donors during bariatric surgery [3]. PTEN haploinsufficient lipoma cells (LipPD1) were obtained from a pediatric PHTS patient [2]. Isolation and culture was performed as previously described [2,17].

2.4. Small-interfering RNA (siRNA) mediated knockdown of SMIM10L1 and PTEN

APCs were seeded at a density of 1,400 cells/cm^2 one day prior to transfection. The transfection was performed using the NEON transfection system (Invitrogen, Thermo Fisher Scientific, Inc) as previously described [3]. Cell pellets were mixed with a combination of two *SMIM10L1* siRNAs (ID #269721, #276961, both Ambion) or two *PTEN* siRNAs (s325, s326, both Ambion) or control siRNA (Silencer™ Negative Control No. 1 siRNA, Ambion). Cells were seeded at a density of 60,000 cells/well on 6-well plates and harvested after 24 h. *SMIM10L1* and *PTEN* knockdown efficiencies were determined via qPCR assays.

2.5. Determination of proliferation

After transfection, cells were seeded at a density of 2,000 cells/well on 96-well plates. *SMIM10L1* knockdown and control APCs were fixed at day 1 and day 7. The medium was renewed every 72 h. Nuclei of fixed cells were stained with Hoechst 33342 (Sigma, Munich, Germany) for 5 min at a concentration of 1 μg/ml in DPBS and fluorescence was measured at 455 nm.

Ki-67 immunofluorescence staining was performed as previously described [3]. The proliferative fraction was defined as Ki-67 positive cells per total nuclei count in %.

Proliferating-Cell-Nuclear-Antigen (PCNA) expression in APCs with and without *SMIM10L1* knockdown was determined via qPCR. Cells were seeded at a density of 60,000 cells/well on 6-well plates and harvested after 24 h.

To investigate *SMIM10L1* knockdown stability, cells with and without *SMIM10L1* knockdown were seeded at a density of 10,000 cells/well on 6-well plates and cultured for 7 days.

2.6. Adipocyte differentiation assays

Cells were seeded in culture medium at a density of 15,000 cells/well on 96-well plates. After 24 h medium was replaced by differentiation medium (Dulbecco's modified Eagle's medium/F12 containing 8 mg/ml D-biotin, 10 mg/ml D-pantothenic acid, 2 μM rosiglitazone, 25 nM dexamethasone, 0.5 mM methylisobuthylxantine, 0.1 μM cortisol, 0.01 mg/ml apotransferrin, 0.2 nM triiodotyronin, and 20 nM human insulin [18]). After 8 days, cells were fixed, stained with Nile Red lipid stain (0.5 μg/ml) and Hoechst 33342 DNA stain (1 μg/ml) and analyzed as described elsewhere [3].

To mimic *in vivo* conditions more closely, a modified method according to Klingelhutz et al. was used for scaffold-free 3D cultures of lipoma cells [19,20]. To form spheroids, 10,000 cells/well were seeded into low attachment 96-well microplates (PS, U-bottom, clear, cellstar®, cell-repellent surface, Greiner Bio-One, Kremsmünster, Austria). Medium was changed to 100 μl differentiation medium after 24 h (day 0). Half of the medium was replaced every 48 h and cells were kept in differentiation medium until day 8. Microscope images were taken daily using the EVOS FL Auto 2 Cell Imaging System (Invitrogen; Thermo Fisher Scientific, Inc). To determine spheroid size, image analysis was performed using ImageJ [21].

To investigate *adiponectin (ADIPOQ)* and *fatty acid binding protein 4* (*FABP4*) as well as *SMIM10L1* mRNA expression during differentiation, APCs with or without *SMIM10L1* knockdown were seeded at a density of 120,000 cells/well on 12-well plates and kept in differentiation medium for 8 days.

SMIM10L1 expression during adipogenesis was determined via qPCR. 130,000 cells/well were seeded on 12-well plates and

medium was replaced by differentiation medium after 24h. Cells were kept in differentiation medium for 4, 8 and 12 days.

Medium for control APCs was replaced by serum-free medium after 24 h. Control cells were harvested after 4 days.

2.7. Quantitative real-time PCR (qPCR)

RNA isolation, reverse transcription and qPCRs were performed as described earlier [17]. TaqMan™ assays were performed using Takyon Low Rox Probe MasterMix dTTP Blue (Eurogentec). For SYBR Green assays we used the Takyon Low Rox SYBR MasterMix dTTP Blue (Eurogentec). Supplement table 1 contains a list of primers used for qPCR assays. Expression was normalized to *hypoxanthine phosphoribosyltransferase* (*HPRT*) and *TATA-box binding protein* (*TBP*).

2.8. Western blot analysis

Cells were seeded at a density of 60,000 cells/well on 6-well plates and changed to serum-free medium after 24 h. Cells were harvested the next day. After lysis and protein extraction, 10 μg protein per lane was separated electrophoretically and blotted onto nitrocellulose membranes as described earlier [2]. Supplement table 2 contains a list of primary (Cell Signaling Technology) and secondary antibodies (Dako; Agilent Technologies). Glyceraldehyde-3-phosphate dehydrogenase (GAPDH) and α-Tubulin were used as loading controls.

2.9. Statistical analysis

Means of ≥ 3 independent experiments were statistically analyzed using GraphPad Prism 6 software (GraphPad Software Inc.). For comparison of two conditions, means of independent experiments were compared via paired Student's t-test. For multiple comparisons, we used one-way analysis of variance (ANOVA) followed by a Tukey's multiple comparisons test. Results are indicated as the mean ± SEM.

3. Results

3.1. SMIM10L1 was significantly downregulated in PTEN knockdown APCs

SMIM10L1 was the most significantly downregulated gene in *PTEN* siRNA knockdown APCs compared to matched controls [3] (Supplementary Fig. 1). We confirmed this via qPCR in APCs, with *PTEN* siRNA knockdown ($p < 0.01$; Fig. 1a). We showed the downregulation of *SMIM10L1* expression to 35.5 ± 1.9% ($p = 0.001$; Fig. 1b), comprising also the coding region of SMIM10L1 (Fig. 1c).

Computational prediction of the 3D structure of the *SMIM10L1* gene product suggests a protein with alpha-helical character. Rosetta was used to scan for the most likely orientation with respect to the membrane. The resulting model matches the Jufo9D secondary structure and membrane position predictions well (Fig. 1d). Two small N-terminal helices are predicted solvent exposed, while the larger C-terminal helix is likely inserted in a membrane. The predicted

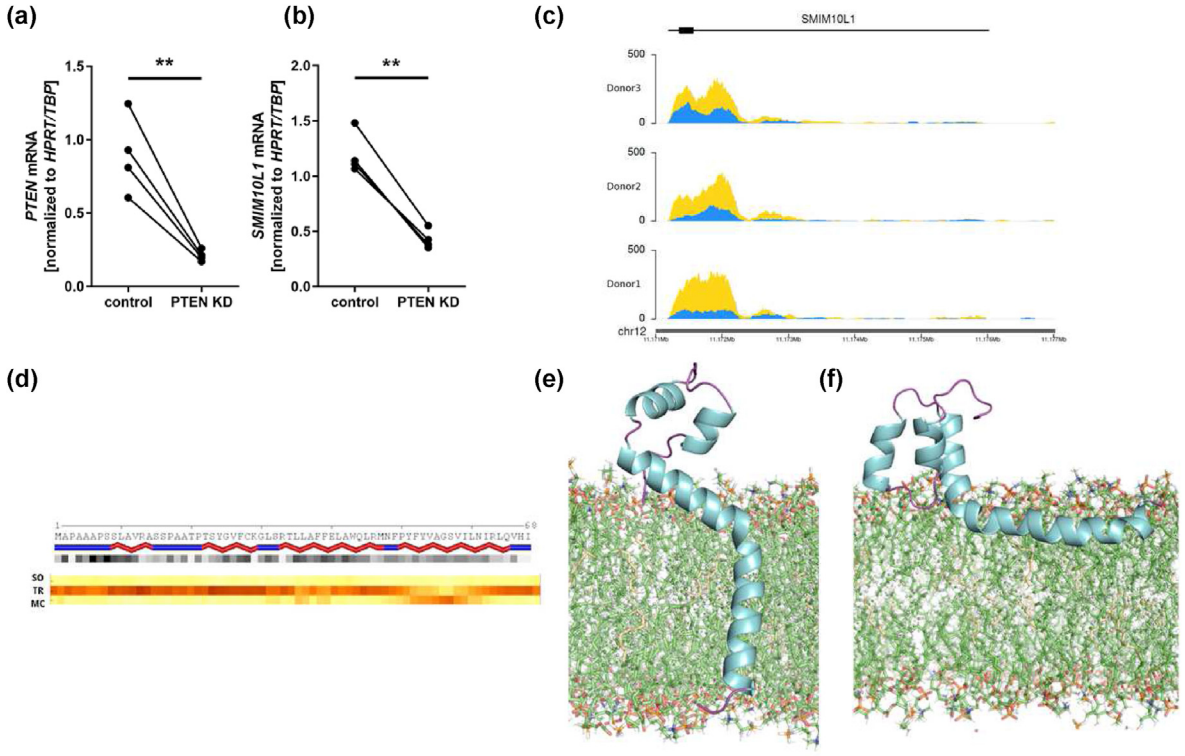

Fig. 1. *SMIM10L1* was downregulated in PTEN knockdown APCs. (a) *PTEN* and **(b)** *SMIM10L1* mRNA expression in control and PTEN siRNA transfected APCs: *PTEN* was knocked down by 75.9 ± 1.5% ($n = 4$, $p = 0.0093$) and was associated with a downregulation of *SMIM10L1* mRNA gene expression by 64.5 ± 1.9% ($n = 4$, $p = 0.001$). **(c)** RNA sequencing data of *SMIM10L1* expression in control (yellow) and PTEN knockdown (blue) APCs. The location of the *SMIM10L1* exon is shown as black bar on top of the expression plots. **(d)** Computational prediction of the SMIM10L1 structure and its orientation in the membrane. The *ab-inito* model of SMIM10L1 exhibits alpha-helical character (red) connected with loops (blue). Jufo 9D (yellow heatmap) predicts localization of the protein in the transmembrane region (TR), and localization into the membrane core (MC) around residue 55. The computational modelling of the orientation in a membrane using Rosetta suggests two possibly favorable orientations: a vertical integration of the C-terminal helix **(e)** or a horizontally oriented helix associated with a membrane **(f)**. Two smaller helices remain exposed to the solvent in both cases. **$p < 0.01$. (For interpretation of the references to colour in this figure legend, the reader is referred to the Web version of this article.)

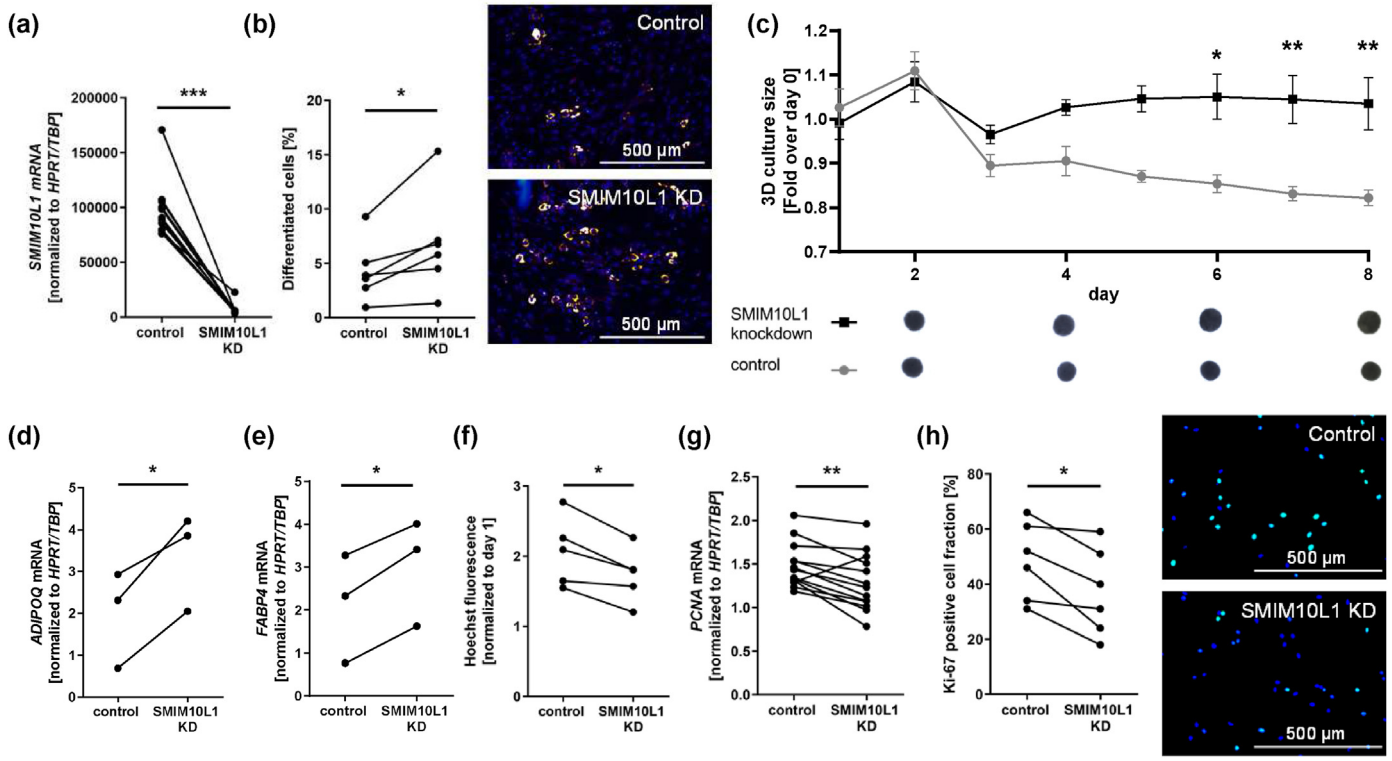

Fig. 2. *SMIM10L1* knockdown enhanced differentiation of APCs. **(a)** mRNA expression of *SMIM10L1* in control and *SMIM10L1* siRNA transfected APCs: *SMIM10L1* was reduced by 92.7 ± 1.9% (n = 13, p < 0.0001). **(b)** Hoechst nuclei staining (blue) and Nile red lipid staining (red) in control and *SMIM10L1* siRNA transfected APCs: the fraction of adipocytes was 1.6 ± 0.2 fold higher in SMIM10L1 knockdown cells compared to controls (n = 7, p < 0.05). **(c)** 3D culture of controls and cells transfected with *SMIM10L1* siRNA: the spheroid size of SMIM10L1 knockdown cells significantly increased during 8 days of differentiation while the size of control spheroids decreased (n = 4). mRNA expression of adipogenesis markers **(d)** *ADIPOQ* and **(e)** *FABP4* in controls and *SMIM10L1* siRNA transfected cells after 8 days of differentiation: *ADIPOQ* mRNA expression in *SMIM10L1* knockdown cells is 204.1 ± 49.6% higher than in controls. (n = 3, p = 0.0378). *FABP4* expression is raised by 60.5 ± 27.0% (n = 3, p = 0.0131) compared to control APCs. **(f)** Hoechst nuclei staining of control and *SMIM10L1* siRNA transfected cells (day 7 over day 1): proliferation in *SMIM10L1* knockdown cells was reduced by 15.8 ± 3.1% (n = 5, p = 0.0115). **(g)** mRNA expression of proliferation marker *PCNA* in controls and *SMIM10L1* siRNA transfected cells: *SMIM10L1* knockdown cells express 13.7 ± 4.1% (n = 13, p = 0.0036) less *PCNA* mRNA than controls. **(h)** Proliferation marker Ki-67 immunofluorescence staining (Ki67 (green)/Hoechst (blue) cell count = proliferative fraction in %) in control and *SMIM10L1* siRNA transfected cells: the proliferative fraction was reduced to 0.8 ± 0.07 fold in SMIM10L1 knockdown cells compared to controls (n = 6, p < 0.05). *p < 0.05, **p < 0.01, ***p < 0.001. (For interpretation of the references to colour in this figure legend, the reader is referred to the Web version of this article.)

Rosetta energy units (REU) are similar and suggest two possible orientations of the C-terminal helix: a vertical integration of the helix into the membrane (Fig. 1e) with −110 REU or a horizontal membrane association (Fig. 1f) with −121 REU.

3.2. SMIM10L1 knockdown enhanced adipocyte differentiation of APCs

To test the effects of *SMIM10L1* downregulation in APCs, we established an efficient siRNA-mediated *SMIM10L1* knockdown (p < 0.0001, Fig. 2a). This knockdown was stable during 7 days of proliferation and 8 days of differentiation (Supplementary Fig. 2). We analyzed SMIM10L1s role in adipogenesis by investigating the effect of *SMIM10L1* downregulation on adipocyte differentiation of APCs. The fraction of adipocytes was significantly increased in SMIM10L1 knockdown cells (p < 0.05; Fig. 2b). Furthermore, we observed that *SMIM10L1* downregulation in a 3D adipogenesis assay led to an increased spheroid size and lipid accumulation compared to spheroids from control APCs (p < 0.01; Fig. 2c). We additionally analyzed gene expression of two adipogenesis markers: *adiponectin* and *FABP4* and detected a significantly higher expression in APCs with *SMIM10L1* knockdown. The expression of *adiponectin* was twice as high as in controls (p < 0.05; Fig. 2d). *FABP4* expression was raised by 60.5 ± 27.0% (<0.05; Fig. 2e).

We analyzed *SMIM10L1* expression at day 0, 4, 8 and 12 of differentiation in APCs and PHTS lipoma (LipPD1) cells. *SMIM10L1* was upregulated during adipogenesis (compared to day 0, p < 0.05) (Supplementary Fig. 3a).

We observed a slight, but significant decrease of proliferation of *SMIM10L1* knockdown APCs (p < 0.05; Fig. 2f). Proliferation marker *PCNA* gene expression was reduced by 13.7 ± 4.1% (p < 0.01; Fig. 2g) and the proliferative fraction of Ki-67 positive cells was reduced to 0.8 ± 0.07 fold in SMIM10L1 knockdown cells compared to controls cells (p < 0.05; Fig. 2h).

3.3. SMIM10L1 enhanced PI3K/AKT/mTOR pathway signaling via PTEN downregulation

In further experiments, we analyzed *PTEN* gene expression in *SMIM10L1* knockdown APCs and noticed that *PTEN* expression was downregulated by 12.7 ± 2.8% (p < 0.01; Fig. 3a). We also saw a downregulation of PTEN protein by 18.9 ± 7.0% in *SMIM10L1* knockdown cells compared to controls (p < 0.05; Fig. 3b).

Interestingly, we found that in *SMIM10L1* siRNA knockdown APCs phosphorylation of AKT was 90.0 ± 18.5% higher than in control cells (p = 0.11; Fig. 3c). AKT activation leads to increased expression of the adipogenic transcription factor sterol regulatory element-binding protein 1 (SREBP1). Consistently, we observed a tendency of increased SREBP1 expression in

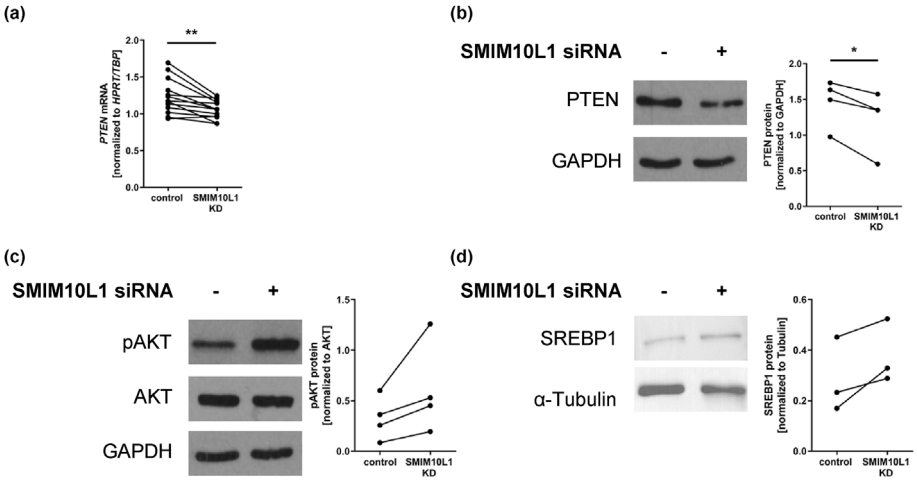

Fig. 3. SMIM10L1 enhanced AKT phosphorylation. **(a)** PTEN mRNA expression in control and SMIM10L1 siRNA transfected cells: PTEN expression is downregulated by 12.7 ± 2.8% (n = 13, p = 0.0018) in SMIM10L1 knockdown cells compared to controls. Western blot of control and SMIM10L1 siRNA transfected cells: a downregulation of SMIM10L1 in APCs using siRNA leads to **(b)** a downregulation of PTEN protein expression by 18.9 ± 7.0% (n = 4, p = 0.0225), **(c)** increased phosphorylation of AKT by 90.0 ± 18.5% (n = 4, p = 0.1132) and **(d)** increased SREBP1 protein expression by 44.4 ± 24.6% (n = 3, p = 0.0961) in SMIM10L1 knockdown cells compared to controls. *p < 0.05, **p < 0.01, ***p < 0.001.

SMIM10L1 knockdown APCs compared to controls (p = 0.096; Fig. 3d).

4. Discussion

Multiple lipomas are frequently observed in pediatric patients with PTEN germline pathogenic variants. The reason and underlying mechanisms behind this adipose tissue dysfunction are not yet clarified. In this study we characterized the role of SMIM10L1 in adipocyte progenitors and investigated whether SMIM10L1 has an impact on adipocyte differentiation. We created a computational prediction of SMIM10L1 three-dimensional structure and found that the small N-terminal helices are probably solvent exposed, while the larger C-terminal helix is likely inserted in a membrane. The *SMIM10L1* gene product is 66% identical to SMIM10 in the C-terminal helix region, which is vertically orientated in the membrane [6].

We found *SMIM10L1* differentially expressed in a data set comparing gene expression in immortalized inguinal vs. epididymal adipose progenitor mouse cell lines during adipocyte differentiation [15] (Supplementary Fig. 3b). In agreement with our study upregulation of *SMIM10L1* during adipogenesis was shown, supporting a role of SMIM10L1 in adipose tissue development.

PTEN downregulation, as observed in PHTS lipoma cells [17], leads to an enhanced proliferation of APCs and confers long-term ability to differentiate into adipocytes, as it has been shown previously [3]. We therefore investigated the impact of *SMIM10L1* downregulation on proliferation and differentiation of APCs. Our data showed that *SMIM10L1* downregulation reduced proliferation but enhanced adipocyte differentiation of adipose progenitors after long-term culture. The reduction in proliferation is not consistent with the increased proliferation observed in APCs with PTEN knockdown [3]. This suggests that SMIM10L1 may not contribute to the enhanced proliferation in PTEN knockdown cells, but plays a specific role in adipocyte differentiation, which could possibly redound to the lipoma formation of patients with PTEN germline pathogenic variants.

Interestingly, we noticed that *PTEN* mRNA and protein expressions were downregulated in *SMIM10L1* knockdown APCs. A possible explanation for this observation might be a so far unknown regulatory crosstalk between PTEN and SMIM10L1. PTEN plays a significant role in the glycolysis, gluconeogenesis, lipid metabolism and mitochondrial metabolism [22]. A mutual interaction between SMIM10L1 and PTEN is not described yet but would be conceivable considering the wide range of PTEN's functions and interaction partners.

In *SMIM10L1* knockdown cells we observed an increased AKT phosphorylation. This could be mediated by the decreased PTEN levels in cells with *SMIM10L1* downregulation. Higher AKT activation could entail the higher SREBP1 protein levels, and consequently increased adipogenesis observed in *SMIM10L1* knockdown cells. Further experimental investigations are needed to detect the mechanisms behind these observed effects and identify possible interaction partners of SMIM10L1.

The present study was designed to investigate the role of SMIM10L1 in adipocyte development and to observe whether SMIM10L1 is involved in mechanisms contributing to the lipoma formation in PHTS patients. We found that SMIM10L1 enhances differentiation of APCs. *SMIM10L1* expression seems to be associated with PTEN gene and protein expression and influences the PI3K/AKT/mTOR signaling pathway. We established a computational prediction of SMIM10L1 and its orientation in the membrane. Further research is needed to better understand the function of SMIM10L1 in adipose tissue development.

Declaration of competing interest

The authors declare no conflicts of interest. The funder had no role in the design of the study; in the collection, analyses, or interpretation of data; in the writing of the manuscript; or in the decision to publish the article.

Acknowledgments

We gratefully acknowledge Sandy Richter for technical assistance and Janine Obendorf and Sören Pietsch for the support with ImageJ. We thank the donors of adipose tissue and Prof. Arne Dittrich for provision.

This study was funded by the German Research Foundation (DFG) - SFB 1052–209933838 Project numbers B10 (M N., J.L., D.L.D., W.K., A.G., A.S.K.), C8 (J.M.), Z4 (S.K., P.F.S.), Z6 (J.M.) and Z2 (open access publishing).

Appendix A. Supplementary data

Supplementary data to this article can be found online at https://doi.org/10.1016/j.bbrc.2022.03.014.

References

[1] L. Yehia, E. Keel, C. Eng, The clinical spectrum of PTEN mutations, Annu. Rev. Med. 71 (2020) 103–116, https://doi.org/10.1146/annurev-med-052218-125823.

[2] G.L. Schmid, F. Kässner, H.H. Uhlig, A. Körner, J. Kratzsch, N. Händel, et al., Sirolimus treatment of severe PTEN hamartoma tumor syndrome: case report and in vitro studies, Pediatr. Res. 75 (4) (2014) 527–534, https://doi.org/10.1038/pr.2013.246.

[3] A.S. Kirstein, S. Kehr, M. Nebe, M. Hanschkow, L.A.G. Barth, J. Lorenz, et al., PTEN regulates adipose progenitor cell growth, differentiation, and replicative aging, J. Biol. Chem. 297 (2) (2021) 100968, https://doi.org/10.1016/j.jbc.2021.100968.

[4] Database GHG, SMIM10L1 gene - GeneCards, SIML1 Protein | SIML1 Antibody. [September 09, 2021]; Available from: https://www.genecards.org/cgi-bin/carddisp.pl?gene=SMIM10L1.

[5] SMIM10L1 protein expression summary - the Human Protein Atlas [September 09, 2021]; Available from: https://www.proteinatlas.org/ENSG00000256537-SMIM10L1.

[6] S. Lubrano, L. Comelli, C. Piccirilli, A. Marranci, F. Dapporto, E. Tantillo, et al., Development of a yeast-based system to identify new hBRAFV600E functional interactors, Oncogene 38 (8) (2019) 1355–1366, https://doi.org/10.1038/s41388-018-0496-5.

[7] C.-Y. Li, G.-Y. Liang, W.-Z. Yao, J. Sui, X. Shen, Y.-Q. Zhang, et al., Integrated analysis of long non-coding RNA competing interactions reveals the potential role in progression of human gastric cancer, Int. J. Oncol. 48 (5) (2016) 1965–1976, https://doi.org/10.3892/ijo.2016.3407.

[8] V. Yarov-Yarovoy, J. Schonbrun, D. Baker, Multipass membrane protein structure prediction using Rosetta, Proteins 62 (4) (2006) 1010–1025, https://doi.org/10.1002/prot.20817.

[9] F. Berenger, R. Shrestha, Y. Zhou, D. Simoncini, K.Y.J. Zhang, Durandal: fast exact clustering of protein decoys, J. Comput. Chem. 33 (4) (2012) 471–474, https://doi.org/10.1002/jcc.21988.

[10] A. Leaver-Fay, M. Tyka, S.M. Lewis, O.F. Lange, J. Thompson, R. Jacak, et al., ROSETTA3: an object-oriented software suite for the simulation and design of macromolecules, Methods Enzymol. 487 (2011) 545–574, https://doi.org/10.1016/B978-0-12-381270-4.00019-6.

[11] J.K. Leman, R. Mueller, M. Karakas, N. Woetzel, J. Meiler, Simultaneous prediction of protein secondary structure and transmembrane spans, Proteins 81 (7) (2013) 1127–1140, https://doi.org/10.1002/prot.24258.

[12] A.A. Porollo, R. Adamczak, J. Meller, POLYVIEW: a flexible visualization tool for structural and functional annotations of proteins, Bioinformatics 20 (15) (2004) 2460–2462, https://doi.org/10.1093/bioinformatics/bth248.

[13] S. Jo, T. Kim, V.G. Iyer, W. Im, CHARMM-GUI: a web-based graphical user interface for CHARMM, J. Comput. Chem. 29 (11) (2008) 1859–1865, https://doi.org/10.1002/jcc.20945.

[14] B.A. Wilson, A. Ramanathan, C.F. Lopez, Cardiolipin-dependent properties of model mitochondrial membranes from molecular simulations, Biophys. J. 117 (3) (2019) 429–444, https://doi.org/10.1016/j.bpj.2019.06.023.

[15] J. Breitfeld, S. Kehr, L. Müller, P.F. Stadler, Y. Böttcher, M. Blüher, et al., Developmentally driven changes in adipogenesis in different fat depots are related to obesity, Front. Endocrinol. 11 (2020) 138, https://doi.org/10.3389/fendo.2020.00138.

[16] B. Gel, E. Serra, karyoploteR: an R/Bioconductor package to plot customizable genomes displaying arbitrary data, Bioinformatics 33 (19) (2017) 3088–3090, https://doi.org/10.1093/bioinformatics/btx346.

[17] F. Kässner, A. Kirstein, N. Händel, G.L. Schmid, K. Landgraf, A. Berthold, et al., A new human adipocyte model with PTEN haploinsufficiency, Adipocyte 9 (1) (2020) 290–301, https://doi.org/10.1080/21623945.2020.1785083.

[18] P. Fischer-Posovszky, F.S. Newell, M. Wabitsch, H.E. Tornqvist, Human SGBS cells - a unique tool for studies of human fat cell biology, Obes Facts 1 (4) (2008) 184–189, https://doi.org/10.1159/000145784.

[19] A.J. Klingelhutz, Scaffold-free generation of uniform adipose spheroids for metabolism research and drug discovery, Sci. Rep. 8 (1) (2018) 1–12, https://doi.org/10.1038/s41598-017-19024-z.

[20] A.S. Kirstein, A. Augustin, M. Penke, M. Cea, A. Körner, W. Kiess, et al., The novel phosphatidylinositol-3-kinase (PI3K) inhibitor alpelisib effectively inhibits growth of PTEN-haploinsufficient lipoma cells, Cancers 11 (10) (2019), https://doi.org/10.3390/cancers11101586.

[21] C.A. Schneider, W.S. Rasband, K.W. Eliceiri, NIH Image to ImageJ: 25 years of image analysis, Nat. Methods 9 (7) (2012) 671–675, https://doi.org/10.1038/nmeth.2089.

[22] C.-Y. Chen, J. Chen, L. He, B.L. Stiles, PTEN: tumor suppressor and metabolic regulator, Front. Endocrinol. 9 (2018) 338, https://doi.org/10.3389/fendo.2018.00338.